ARTICLE TYPE

Impact of B_0 field imperfections correction on BOLD sensitivity in 3D-SPARKLING fMRI data

Zaineb Amor[1] | Caroline Le Ster[1] | Chaithya G R[1,2] | Guillaume Daval-Frérot[1,2,3] | Nicolas Boulant[1] | Franck Mauconduit[1] | Bertrand Thirion[1,2] | Philippe Ciuciu[1,2] | Alexandre Vignaud[1]

[1]Université Paris-Saclay, CEA, NeuroSpin, CNRS, Gif-sur-Yvette, France
[2]Inria, MIND, Palaiseau, France
[3]Siemens Healthineers, Courbevoie, France

Correspondence
Alexandre Vignaud. Email: Alexandre.Vignaud@cea.fr

Present Address
CEA Saclay, NeuroSpin, Bâtiment 145, Gif-sur-Yvette, France.

Funding Information
Chaithya G R was supported by the CEA NUMERICS program, which has received funding from the European Union's Horizon 2020 research and innovation program under the Marie Sklodowska-Curie grant agreement No 800945. This work was granted access to the HPC resources of TGCC in France under the allocation 2019-GCH0424 made by GENCI. This work has received financial support from Leducq Foundation (Large Equipement de Recherche et Plateformes Technologiques program).

Purpose: Static and dynamic B_0 field imperfections are detrimental to functional MRI (fMRI) applications, especially at ultra-high magnetic fields (UHF). In this work, a field camera is used to assess the benefits of retrospectively correcting B_0 field perturbations on Blood Oxygen Level Dependent (BOLD) sensitivity in non-Cartesian 3D-SPARKLING fMRI acquisitions.

Methods: FMRI data was acquired at 1mm^3 and for a 2.4s-TR while concurrently monitoring in real-time field perturbations using a Skope Clip-on field camera in a novel experimental setting involving a shorter TR than the required minimal TR of the field probes. Measurements of the dynamic field deviations were used along with a static ΔB_0 map to retrospectively correct static and dynamic field imperfections, respectively. In order to evaluate the impact of such a correction on fMRI volumes, a comparative study was conducted on healthy volunteers.

Results: Correction of B_0 deviations improved image quality and yielded between 20% and 30% increase in median temporal signal-to-noise ratio (tSNR). Using fMRI data collected during a retinotopic mapping experiment, we demonstrated a significant increase in sensitivity to the BOLD contrast and improved accuracy of the BOLD phase maps: 44% (resp., 159%) more activated voxels were retrieved when using a significance control level based on a p-value of 0.001 without correcting for multiple comparisons (resp., 0.05 with a false discovery rate correction).

Conclusion: 3D-SPARKLING fMRI hugely benefits from static and dynamic B_0 imperfections correction. However, the proposed experimental protocol is flexible enough to be deployed on a large spectrum of encoding schemes, including arbitrary non-Cartesian readouts.

Total number of words and figures/tables: : 5226 words and 9 Figures/Tables

KEYWORDS:
fMRI, B_0 inhomogeneities, NMR probes, Field monitoring, non-Cartesian, 3D-SPARKLING

Received: 00 Month 0000 | Revised: 00 Month 0000 | Accepted: 00 Month 0000

DOI: xxx/xxxx

SUPPORTING INFORMATION

The following supporting information is available as part of the online article:

Section S1 Reconstruction pipeline.
Section S2 Summary of the different reconstruction strategies.
Section S3 Power spectra of physiological noise-induced field perturbations.
Section S4 Time course of motion regressors of the translation over the z-axis (estimated with SPM12) for volunteer#3 and the three physiological noise scenarios.
Section S5 Time course of motion regressors of the translation over the z-axis (estimated with SPM12) for the three volunteers and the clockwise as well as the counter-clockwise time series data.
Section S6 Prescribed versus measured trajectories.
Table S1 Table summarizing the different reconstruction strategies and the impact on the reconstruction algorithm with respect to the terms included in the signal model and reconstruction time.
Figure S1 (A) Power spectra of the $\Delta B_{0,dyn}$ term monitored during resting-state fMRI for the 3 volunteers and (B) for the volunteer#3 at the different physiological noise scenarios. Only the range [0.12Hz, 0.4Hz] is displayed to observe the fluctuations due to breathing.
Figure S2 Time course of motion regressors of the translation over the z-axis (estimated with SPM12) for volunteer#3 and the three physiological noise scenarios.
Figure S3 Time course of motion regressors of the translation over the z-axis (estimated with SPM12) for the three volunteers and the clockwise as well as the counter-clockwise time series data.
Figure S4 Prescribed versus measured trajectories: Three randomly chosen prescribed shots (in blue) and plotted against the corresponding measured trajectories (in black) (A) in 3D and (B) along each of the three axes.

Section S1 Reconstruction pipeline

Each volume ($\boldsymbol{x}_j \in \mathbb{C}^N, j = 1,..,N_t$) is reconstructed independently from the others through the CS-based reconstruction solving the problem is Eq. (1) where $\widetilde{\boldsymbol{y}}_{j,\ell} = [\widetilde{\mu}_{\ell,1},\dots,\widetilde{\mu}_{\ell,N_{shot}}]+\boldsymbol{n}_{j,\ell}$ is the k-space data, associated with the set of sampled frequencies points $\widetilde{\Omega}_j = \widetilde{\Omega} = [\widetilde{\boldsymbol{k}}_1,\dots,\widetilde{\boldsymbol{k}}_{N_{shot}}]$ relative to the j-th volume. Here, $\boldsymbol{n}_{j,\ell}$ is additive zero mean white Gaussian noise of σ_ℓ^2 variance and $\widetilde{\boldsymbol{y}}_{j,\ell} \in \mathbb{C}^M$. N and M are, respectively, the number of voxels in each volume and that of the k-space measurements collected by each coil. $\boldsymbol{S}_\ell$ denotes the sensitivity profile of the ℓ-th coil and $\widetilde{\boldsymbol{F}}_{P,\widetilde{\Omega}}$ the *linearized over P interpolators* off-resonance corrected Fourier operator. $\boldsymbol{\Psi}$ is the sym8 wavelet sparsifying basis, g is chosen as the ℓ_1-norm, and the other reconstruction parameters were set to $L = 32$, $P = 30$, $\lambda = 10^{-8}$.

$$\hat{\boldsymbol{x}}_j = \underset{\boldsymbol{x}_j \in \mathbb{C}^N}{\arg\min} \frac{1}{2} \sum_{\ell=1}^{L} \sigma_\ell^{-2} \left\| \widetilde{\boldsymbol{F}}_{P,\widetilde{\Omega}} \boldsymbol{S}_\ell \boldsymbol{x}_j - \tilde{\boldsymbol{y}}_{j,\ell} \right\|_2^2 + \lambda g(\boldsymbol{\Psi}\boldsymbol{x}_j). \quad (1)$$

Additionally, the Siemens scanner applies an eddy current phase compensation upon reception of the raw k-space data $\boldsymbol{y}_{j,\ell} = [\mu_{\ell,1},\dots,\mu_{\ell,N_{shot}}] + \boldsymbol{n}_{j,\ell}$. The field camera does not perform such a correction. Applying the zeroth order dynamic correction on $\boldsymbol{y}_{j,\ell}$ directly using $k_0 = [k_{0,1} \dots k_{0,Nshot}]$ without taking into account this additional step means that eddy currents phase compensation will be applied twice. To avoid this, we cancel the correction applied by the scanner by demodulating the k-space data by a simulated phase of the eddy current compensation before correcting the zeroth order field term. For one full fMRI time series the sizes of the scanner (32-channel data of N= 120 or 125 volumes at 1mm^3) and field monitoring data are, respectively, 20 GB and 13GB. The reconstruction of each full-time series was run on the Jean Zay cluster where every five volumes were parallelized over a single Nvidia V100 GPU, allowing the reconstruction of the full times series in a few hours (3 to 8 depending on the number of GPUs available). On more accessible hardware the reconstruction time is longer:

1. A local cluster with 4 GPU nodes would enable the reconstruction of one fMRI time series in about one day.
2. On a standard machine that has a Quadro RTX 8000 GPU and Intel Xeon Silver 4214 CPU @2.20GHz (12 cores and 24 threads) and using a simple embarrassingly parallel pipeline by launching six reconstructions at once using joblib*, the reconstruction time is of about 4 days.

Following the recent in-house developments † and further optimizing the CUFI-NUFFT‡ implementation in 3D can help to reduce the reconstruction time in the future. Furthermore, the reconstruction algorithm currently has many GPU/CPU transfers due to the lack of GPU implementation of the wavelet transform. If the latter was available, such transfers would be significantly reduced, hence the reconstruction time would be much shorter. These issues will be handled in the near future.

Section S2 Summary of the different reconstruction strategies

Table S1 Table summarizing the different reconstruction strategies and the impact on the reconstruction algorithm

*https://joblib.readthedocs.io/en/stable/
†https://github.com/mind-inria/mri-nufft
‡https://github.com/flatironinstitute/cufinufft

with respect to the terms included in the signal model and reconstruction time.

Section S3 Power spectra of physiological noise-induced field perturbations

Figure S1 (A) Power spectra of the $\Delta B_{0,dyn}$ term monitored during resting-state fMRI for the 3 volunteers and (B) for the volunteer#3 at the different physiological noise scenarios. Only the range [0.12Hz, 0.4Hz] is displayed to observe the fluctuations due to breathing.

Section S4 Time course of motion regressors of the translation over the z-axis (estimated with SPM12) for volunteer#3 and the three physiological noise scenarios.

Figure S2 Time course of motion regressors of the translation over the z-axis (estimated with SPM12) for volunteer#3 and the three physiological noise scenarios..

S5 Time course of motion regressors of the translation over the z-axis (estimated with SPM12) for the three volunteers and the clockwise as well as the counter-clockwise time series data

Figure S3 Time course of motion regressors of the translation over the z-axis (estimated with SPM12) for the three volunteers and the clockwise as well as the counter-clockwise time series data.

Section S6 Prescribed versus measured trajectories

In Fig. S4-(A), we show three randomly chosen shots out of the 48 shots used in a volumetric TR (the 5th, 16th, and 27th shots). The prescribed (theoretical) trajectories are plotted in blue, whereas those measured during the 20th repetition of the resting-state fMRI scans acquired from V#1 are drawn in black. The 20th repetition is taken as an example. The results are similar across all repetitions. We observe a good agreement between the prescribed trajectories and the actual ones. This is confirmed when looking more closely at the 16th shot in Fig. S4-(B) over the three axes: The k-space locations were normalized between -0.5 and 0.5. We quantified the maximum error in k-space location, on this resting-state data set, as 1% relative to k_{max}. Therefore, the zeroth order captures most of the dynamic field perturbations. Only residual perturbations are captured by the first and higher-order terms. Our results show that the first-order term (errors along the trajectories) has a less significant impact on the tSNR (and therefore on the temporal variance) than the zeroth-order. However, the impact on image quality shows that even such minor discrepancies between the prescribed trajectories and those actually played by the system can impact image quality.

Figure S4 Prescribed versus measured trajectories: Three randomly chosen prescribed shots (in blue) and plotted against the corresponding measured trajectories (in black) (A) in 3D and (B) along each of the three axes.

ORCID

Zaineb Amor https://orcid.org/0000-0002-7776-790X *Caroline Le*

REFERENCES

Table S1 Table summarizing the different reconstruction strategies and the impact on the reconstruction algorithm with respect to the terms included in the signal model and reconstruction time.

	Static contribution: $\Delta B_{0,stat}$		Dynamic contributions: $\Delta B_{0,dyn}$ and $\delta \boldsymbol{k}$				
	Encoding operator		K-space data		Trajectories		Reconstruction
	Fourier	non-Fourier ($\widetilde{\boldsymbol{F}}_P$)	Uncorrected ($\boldsymbol{y}$)	Corrected ($\widetilde{\boldsymbol{y}}$)	Prescribed ($\boldsymbol{\Omega}$)	Measured ($\widetilde{\boldsymbol{\Omega}}$)	time per volume
(a)	×		×		×		∼15min
(b)	×			×	×		∼15min
(c)	×			×		×	∼15min
(d)		×	×		×		∼3h
(e)		×		×	×		∼3h
(f)		×		×		×	∼3h

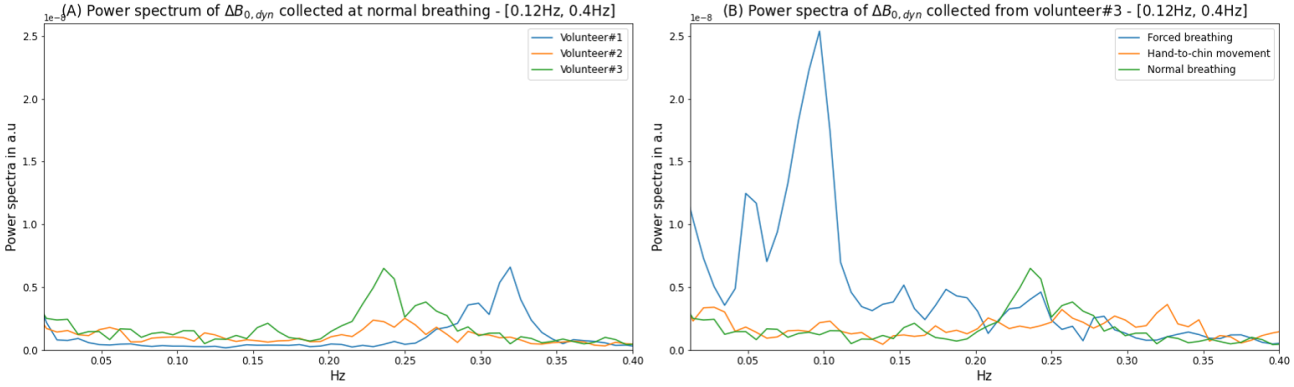

Figure S1 (A) Power spectra of the $\Delta B_{0,dyn}$ term monitored during resting-state fMRI for the 3 volunteers and (B) for the volunteer#3 at the different physiological noise scenarios. Only the range [0.12Hz, 0.4Hz] is displayed to observe the fluctuations due to breathing.

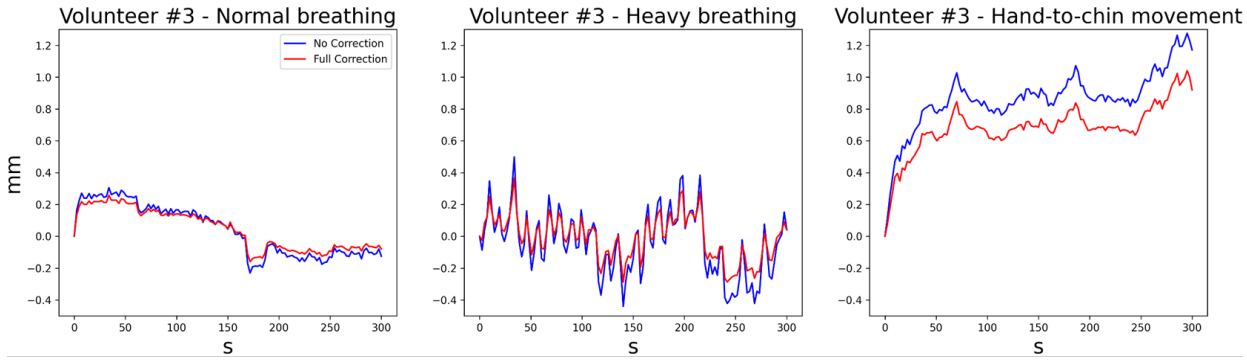

Figure S2 Time course of motion regressors of the translation over the z-axis (estimated with SPM12) for volunteer#3 and the three physiological noise scenarios.

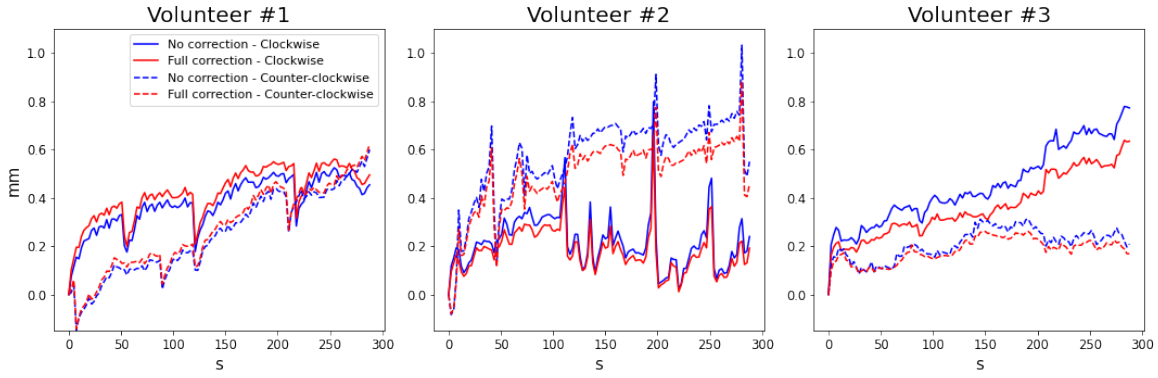

Figure S3 Time course of motion regressors of the translation over the z-axis (estimated with SPM12) for the three volunteers and the clockwise as well as the counter-clockwise time series data.

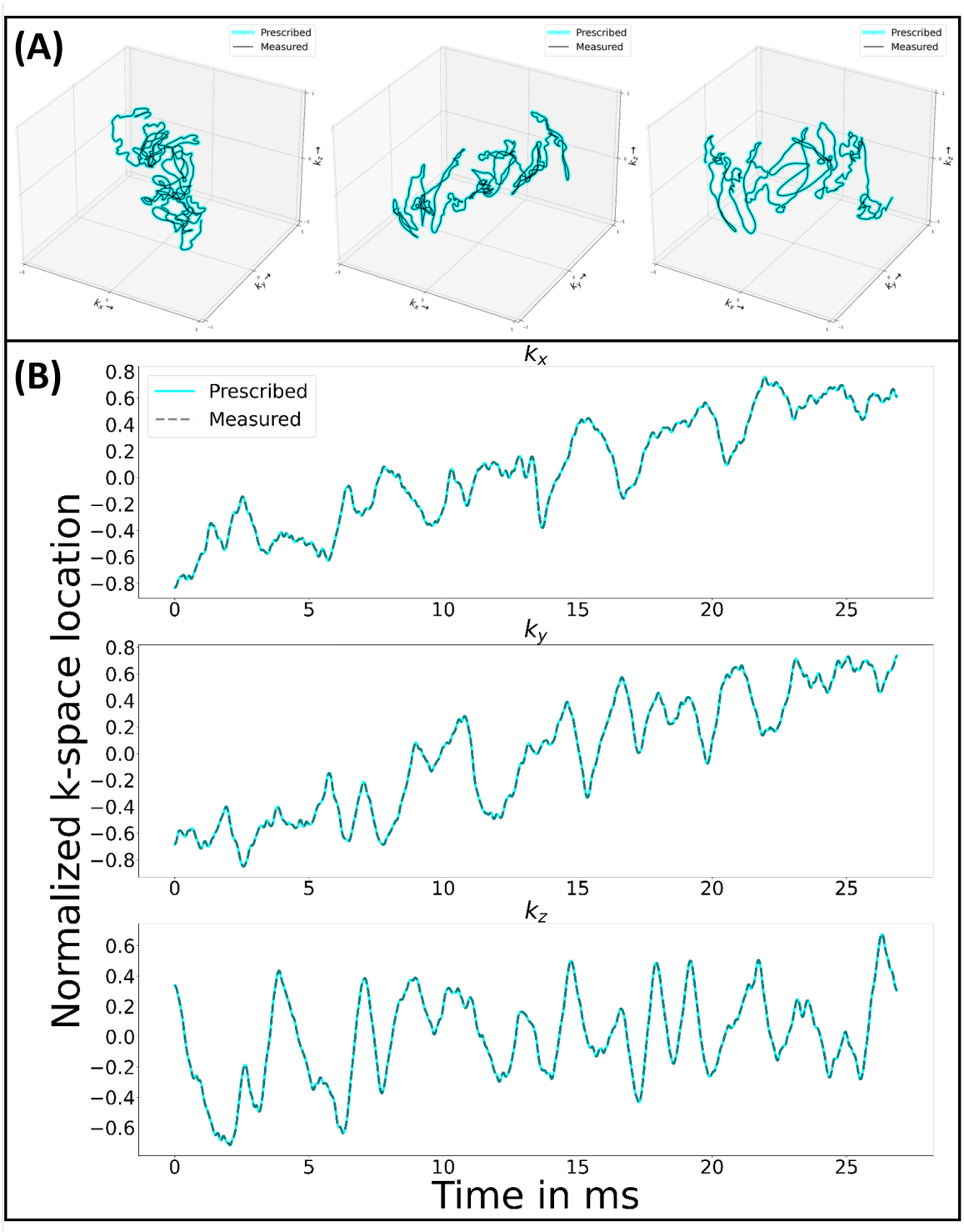

Figure S4 Prescribed versus measured trajectories: Three randomly chosen prescribed shots (in blue) and plotted against the corresponding measured trajectories (in black) (A) in 3D and (B) along each of the three axes.